npj | parkinson's disease

Brief communication

Published in partnership with the Parkinson's Foundation

https://doi.org/10.1038/s41531-024-00850-8

Intracellular α-synuclein assemblies are sufficient to alter nanoscale diffusion in the striatal extracellular space

J. Estaun-Panzano[1], S. Nandi[2,3], Q. Gresil[2,3], E. Doudnikoff[1], C. Mazzocco[1], ML. Arotcarena[1], MH. Canron[1], B. Dehay[1], L. Cognet[2,3] & E. Bezard[1]

α-synucleinopathies progression involves the spread of α-synuclein aggregates through the extracellular space (ECS). Single-particle tracking studies showed that α-synuclein-induced neurodegeneration increases ECS molecular diffusivity. To disentangle the consequences of neuronal loss versus α-synuclein-positive intracellular assemblies formation, we performed near-infrared single-particle tracking to characterise ECS rheology in the striatum of mouse models of α-synucleinopathies. We showed that intracellular α-synuclein assemblies, without neurodegeneration, suffice to alter nanoscale diffusion in the striatal ECS.

It is widely accepted that α-synuclein (α-syn) pathology propagates through interconnected brain regions[1]. Evidence suggests that cell-to-cell propagation occurs, at least in part, via the extracellular space (ECS)[2]. The characterisation[3,4] of this heterogeneous space, made of channels ranging from 20 to 400 nm and filled with a complex extracellular matrix (ECM), is, therefore, crucial as local rheological properties of this environment may influence the spread and development of proteinopathies. Recent studies point to different changes in the ECS/ECM related to α-synucleinopathy[5,6]. Remarkably, Soria et al. reported that α-syn-induced neurodegeneration in the Substantia Nigra pars compacta (SNc)[3,7] is concomitant with matrix disruption and a significant increase in ECS diffusivity[3]. Nonetheless, the question of whether these changes in diffusivity are a direct consequence of (i) neurodegeneration, i.e., the loss of neurons, (ii) intracellular protein aggregates, or (iii) precede those events, potentially facilitating the diffusion of pathological seeds during the prodromal phase of the disease, remains an open question.

Administering patient-derived Lewy bodies (LB) in the SNc induces loss of dopaminergic neurons and an increase in nigral phosphorylated α-syn at Ser129 (p-syn) as a surrogate marker of the presence of α-syn pathology. Still, it does not lead to the production of α-syn aggregates in the striatum[3]. Injecting pre-formed fibrils (PFF) of recombinant α-syn into the SNc leads to prominent striatal α-syn pathology with many intracellular assemblies in medium spiny neurons (MSNs)[7]. The striatum thus displays a strikingly different profile in these two aggregated α-syn trigger modalities that have the additional advantage of the striatal ECS not being compromised by the surgical procedure performed in the SNc.

Since Soria et al. studied the degenerative SNc[3], we first aimed at replicating their baseline values in healthy SNc and at further characterising the diffusive regimes and ECS local widths in the entire healthy nigrostriatal pathway, i.e. SNc, Substantia nigra pars reticulata (SNr) and striatum (Str). For this objective, we used our recently developed single-particle approach with Single-Walled Carbon Nanotubes (SWCNTs) as near-infrared probes in adult mouse brain acute slices[8,9] (Fig. 1a). These probes present typical lengths around 500 nm and diameters, including their surfactant, in the range of 2–5 nm (Supplementary Fig. 1). The reconstructed ECS maps illustrate the heterogeneous nature of the ECS, emphasising the considerable variations in local properties, i.e., *local* diffusivity, defined as normalized instantaneous diffusion coefficients or how fast the particle moves at every spatial point, and channel width at the nano-scale (Fig. 1a)[3,8,9]. Strikingly, ECS presents diverse properties across the nigrostriatal pathway (Fig. 1b, c and Supplementary Fig. 2). The SNc exhibits significantly narrower local sizes and slower diffusions, which is compatible with a region with packed dopaminergic neurons, and is aligned with Soria et al. findings[3]. In contrast, SNr and Str show more heterogeneous distributions with diffusional values compatible with highly restricted diffusion zones coexisting with looser areas displaying relatively high mobility (Fig. 1b) but overall displaying higher values of local diffusivity. The distribution of local channel widths follows the same trend, with notably larger distributions (Fig. 1c). In agreement with the restricted diffusion theory of nanometric objects, higher local channel widths present higher diffusivity properties[10]. Accordingly, we found a positive correlation between ECS dimensions and local diffusivity (Pearson's $r = 0.208$ SNc, 0.401 SNr, 0.330 Str, $p < 0.0001$) (Fig. 1d),

[1]Univ. Bordeaux, CNRS, Institut des Maladies Neurodégénératives, UMR 5293, F-33000 Bordeaux, France. [2]Univ. Bordeaux, CNRS, Laboratoire Photonique, Numérique et Nanosciences, UMR 5298, F-33400 Talence, France. [3]IOGS, CNRS, Laboratoire Photonique, Numérique et Nanosciences, UMR 5298, F-33400 Talence, France. e-mail: erwan.bezard@u-bordeaux.fr

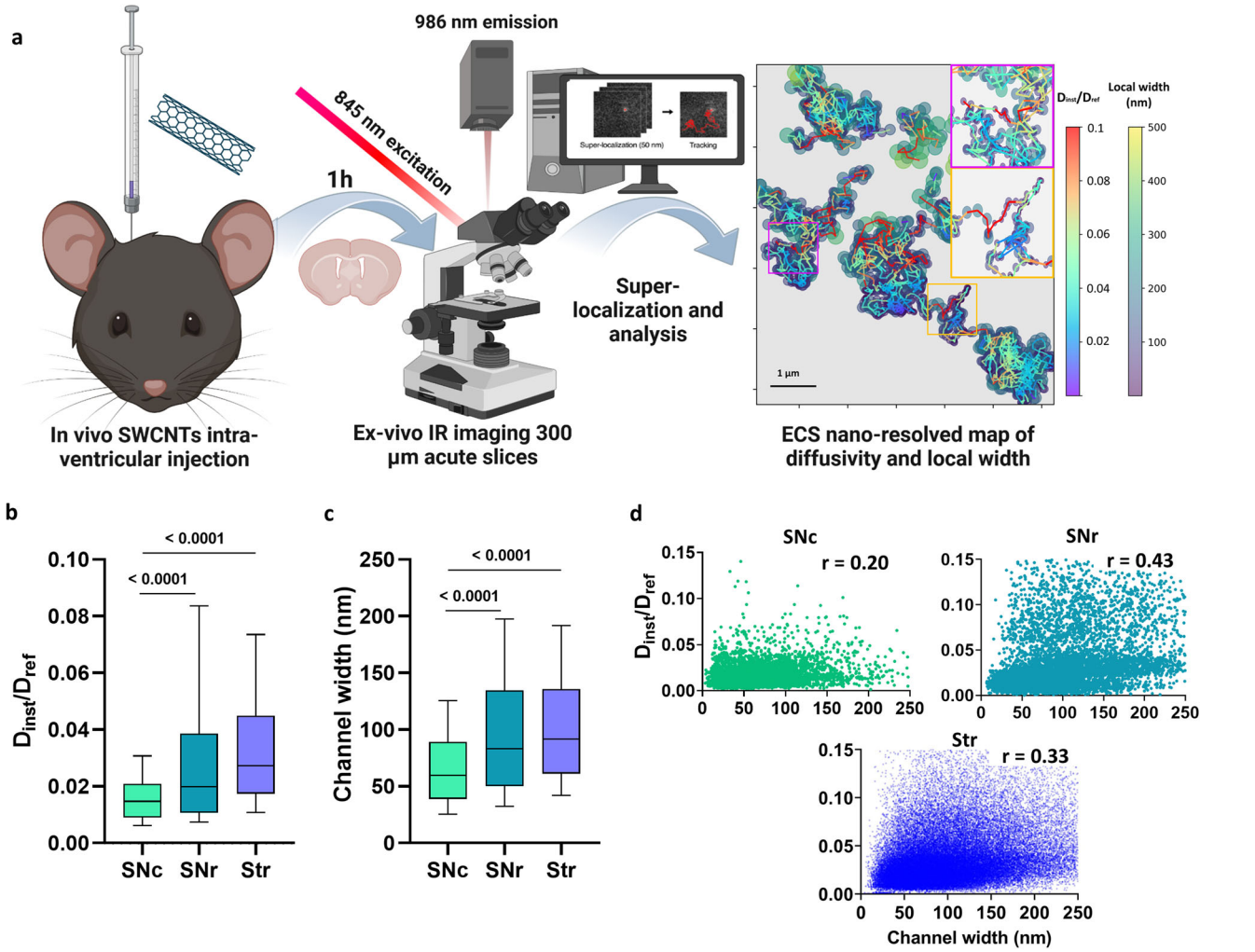

Fig. 1 | The nigro-striatal pathway presents diverse ECS properties and matrix complexity. a SWCNT tracking and analysis experimental workflow. SWCNTs were administered in vivo into the lateral ventricles and allowed to diffuse into the brain for 1 h. Acute brain slices were prepared in ice-cold NMDG-based solution and imaged in aCSF at 35 °C under carbogen bubbling. SWCNTs were excited using an 845 nm laser. Post hoc analysis permitted the super-localization and trajectory reconstruction. Each trajectory provided a local map and distribution of values of local diffusivities (D_{inst}/D_{ref}) and local channel widths. These maps reveal a heterogeneous ECS in the nigro-striatal pathway (SN_c: substantia nigra pars compacta, SNr: substantia nigra pars reticulata, Str: striatum). **b** Distributions of Dinst/Dref values (one-way ANOVA F (2, 77608) = 157.4, *p* value < 0.0001) and **c** Distributions of local ECS widths (nm) values (one-way ANOVA F (2, 77608) = 97.41, *p* value < 0.0001). SNc presents a significantly different diffusion regime and local sizes than SNr and Str. **d** Scatter plots depicting the relationship between channel width and instantaneous diffusion coefficient for each data point ($n = 4$ mice SNc and SNr. $n = 10$ mice Str). *Created in BioRender. Bezard, E. (2023) BioRender.com/i55x918.*

suggesting that ECS diffusion is a multi-factorial-dependent process beyond size, likely influenced by matrix density and composition[11] where high diffusivity points do not necessarily correspond to wider ECS spaces[3].

Next, we investigated the ECS rheology of the striatum of SNc-injected LB and PFF-injected mice generated as previously described[3,7]. Briefly, 2 µL of pathological seeds (either LB extracts or PFF) or sham (PBS) were injected over the right SNc of eight-week-old wild-type C57BL/6Jr mice. Four months post-injection, mice were injected with SWCNT for imaging and tracking in striatum live tissue (Fig. 2a). Parallelly, immunostaining characterization was performed into the striatum. As expected, the ipsilateral side of the PFF mice exhibited a very significant load of p-syn positive intracytoplasmic assemblies into the Str, whereas the other groups did not (Fig. 2b).

Both LB and PFF groups showed a stable number of MSNs (Fig. 2c), an absence of striatal microglial activation (Fig. 2d), and a comparable subtle, but significant, decrease in dopamine terminal innervation (Fig. 2e). In the context of no neurodegeneration or lack of microglial activation, we reasoned that the ECM should be unaffected, at odds with degenerative conditions such as degenerative SNc[3] or in the cortex of APP/PS1 mouse model of Alzheimer's disease. However, since α-syn pathology could cause ECM changes, including altered composition and degradation[5,12], we conducted a quantitative analysis of hyaluronic acid (HA) complexity in the striatum. HA is widely acknowledged as the primary structural component of the extracellular matrix in the brain[13], making it a reliable indicator of matrix complexity. We targeted hyaluronan binding protein (HABP) and examined it through fluorescence confocal microscopy. Specifically, we investigated the fractal dimension of the HABP signal in the ipsilateral and contralateral striatum as a proxy of matrix interconnectivity[3]. Our analysis revealed no significant changes in the HABP area nor complexity of the HA backbone in any group (Fig. 2f, g). Additionally, we assessed potential local HABP structural changes around deposits of α-syn by defining regions of interest (ROIs) with a 15 µm radius around p-syn positive or non-positive cells in the same PFF-injected mice. We found no differences in HABP area or structural integrity around p-syn-positive and negative cells (Fig. 2h–j).

However, in the Str, LB and PFF mice ECS rheology strikingly separated according to the sole load of pathological α-syn-positive assemblies. The channel width showed no difference in LB and PFF mice (Fig. 2k), suggesting the subtle dopaminergic innervation loss did not affect the

striatum's ECS channel dimensions. Conversely, diffusivity was significantly increased in the PFF mice compared to control and LB mice (Fig. 2l), suggesting that p-syn-positive assemblies in a given structure suffice to affect the diffusion of molecules into the ECS without apparent alteration of the ECM backbone. While this variation is notably smaller than those found in neuron-degenerative models[3], it is noteworthy that it manifests in the absence of neuronal death despite the modest dopaminergic innervation loss (but with no difference between the two modelling modalities).

Beyond the HA scaffold, the ECM manifests as a remarkably intricate and dynamic assembly backbone[14]. Although we found no changes in the hyaluronan matrix backbone, accumulating evidence indicates a substantial impact on the levels of ECM components in various neurodegenerative diseases, including Parkinson's disease[5,15]. These ECM components are hypothesised to interact with or process pathological misfolded proteins, potentially changing their properties and thus regulating their spreading capabilities[16]. Recent literature reports that extracellular pathological α-syn

Fig. 2 | Influence of α-synuclein pathology on the striatal ECS. a Model generation: Either PBS, LB extracts, or PFF were injected over the right SNc of wild-type mice. Four months post-injection, mice were used for SWCNT tracking or immunostaining. **b** Quantification of surface-positive phosphorylated α-synuclein at the serine 129. **c** Medium spiny neuron quantified by DARPP-32-positive immunostaining stereological counting. There was no DARPP-32 positive-cell loss in any of the models (Kruskal-Wallis H (2) = 0.78, *p* value = 0.7). **d** The extent of microglial activation was quantified as %ipsi/contra of Iba-1 labelled positive surface. There was no significant difference among groups (Kruskal-Wallis H (2) = 3.90, *p* value = 0.14). **e** Striatal dopamine innervation quantified as %ipsi/contra of Tyrosine hydroxylase (TH) optical density (Kruskal-Wallis H (2) = 7.94, *p* value = 0.01). *n* = 5 mice per group for immunostainings. **f,g** Matrix complexity was quantified in the striatum using total hyaluronan area (Kruskal-Wallis H (5) = 4.97, *p* value = 0.42) and fractal dimension analysis of HABP immunofluorescence staining (Kruskal-Wallis H (5) = 2.38, *p* value = 0.79). Connected points represent the same mouse (*n* = 5 mice per group). **h–j** HABP signal was quantified in ROIs centred around p-S129-α-syn-positive-cells. Neither the % area of HA (i) nor fractal dimension (j) of ROIs around p-syn or non-p-syn showed significant differences (Mann–Whitney test *p* value = 0.70 and 0.54, respectively, *n* = 4 mice). **k** Striatal local ECS width values (nm) derived from SWCNT analyses show non-significant differences among the study groups (one-way ANOVA F (2, 150811) = 2.973, *p* value = 0.18). **l** D_{inst}/D_{ref} values in the striatum of mice obtained from SWCNT diffusion analysis. The PFF-injected group presents a significative increase in diffusivity values (one-way ANOVA F (2, 150811) = 8.488 *p* value = 0.012) (*n* = 10 PBS, PFF, *n* = 4 LB). *Created in BioRender. Bezard, E. (2023) BioRender.com/b68b484.*

can trigger proinflammatory reactions by microglia[2], notably through the release of metalloproteinases, which, in turn, can affect matrix integrity[14,17,18].

Caution is however required when interpreting the present data. First, one should remember that the measurements of extracellular diffusion are probe-dependent, reflecting the behaviour of SWCNTs and similar-sized particles rather than providing a universal measure of ECS diffusivity or exhaustive distribution of sizes. Second, it is possible that, ECS regions with particular geometries, such as the smallest pockets and channels (e.g., synaptic clefts), may not be adequately explored by SWCNTs, leaving a proportion of the ECS "invisible". It is also likely that different objects (i.e., ions or protein oligomers) diffuse fundamentally differently or are affected by diverse factors. Distinct diffusion species and methodologies will thus yield varying results. For example, Cragg and colleagues reported an opposite result to ours regarding the comparative diffusivity between SNc and SNr when using ionic probes and measuring diffusion between two points instead of "mapping" the zone like we do[19]. Here, we present a direct comparison of two biological situations using the very same reporter. Whether these changes are relevant to ions, neurotransmitters, or just bigger objects remains an open question.

This work raises several questions: first, how do ECS and ECM properties affect or limit the transmission and clearance of these seeds? Second, how does the presence of pathological α-syn in the ECS and cells impact the composition and properties of the ECM?[3,20]. Our pioneer nanoscopic observations reveal that (i) commonly affected areas show significantly different diffusivity distributions, probably affecting disease expansion and/or waste-cleaning properties, and (ii) α-syn pathology alone is sufficient to affect the diffusion of molecules within the ECS. Further understanding of the complex interplay between intracellular α-syn pathology and ECS diffusivity may dramatically affect our modelling of α-syn spreading and therapeutic approaches, notably through immunisation strategies.

Methods

Ethics Statement

Experiments were performed following the European Union directive (2010/63/EU) on protecting animals used for scientific purposes. They were approved by the Ethical Committee of Bordeaux University (CEEA 50, France) and the Ministry of Education and Research under license number APAFIS #32540-2021072016125086 v11. The study is reported following ARRIVE guidelines (https://arriveguidelines.org).

Purification of LB from human PD brains

LB purification was conducted as previously described[21]. The samples were obtained from brains collected in a Brain Donation Programme of the Brain Bank "GIE NeuroCEB" run by a consortium of patient associations: ARSEP (association for research on multiple sclerosis), CSC (cerebellar ataxias), France Alzheimer, and France Parkinson. The consent forms were signed by the patients themselves or their next kin in their name, following the French Bioethical Laws. The Brain Bank GIE NeuroCEB (Bioresource Research Impact Factor number BB-0033-00011) has been declared at the Ministry of Higher Education and Research and has received approval to distribute samples (agreement AC-2013-1887). Human SNpc was dissected from fresh frozen postmortem midbrain samples from 5 patients with sporadic PD exhibiting conspicuous LB pathology on neuropathological examination (mean age at death: 67.5 ± 3.5 years; frozen postmortem interval: 17 ± 4 h). Tissue was homogenised in 9 vol (w/v) ice-cold MSE with protease inhibitor cocktail (Complete Mini; Boehringer Mannheim) with 12 strokes of a motor-driven glass/Teflon homogeniser. A sucrose step gradient was prepared for LB purification by overlaying 2.2 M with 1.4 M and finally with 1.2 M sucrose in volume ratios of 3.5:8:8 (v/v) 74. The homogenate was layered on the gradient and centrifuged at 160,000 × *g* for 3 h using an SW32.1 rotor (Beckman). Twenty-six fractions of 500 µl were collected from each gradient from the top (fraction 1) to bottom (fraction 26) and analysed for the presence of α-syn aggregates by filter retardation assay, with 45 µl of each fraction deposited 26. LB-containing fractions from PD patients were those between fractions 21 and 23. The amount of α-syn in the LB fractions was quantified using a human α-syn ELISA kit (#KHB0061; Invitrogen/Life Technologies, Carlsbad, CA, USA). Quantification by ELISA indicated that the LB mix contained 24 pg of α-syn per microliter. Those SN-derived LB fractions have been fully characterised biochemically[21].

α-Syn fibrillisation

Solutions of monomeric α-Syn at 4 to 5 mg/mL in saline (H2O, 100 mM NaCl, and 20 mM tris-HCl pH 7.40) were sterilised by filtration through 0.22 µm Millipore single-use filters and stored in sterile 15 mL conical falcon tubes at 4 °C. Sterilised stock was then distributed into safe-lock Biopur individually sterile-packaged 1.5 mL Eppendorf tubes as 500 µL aliquots and were seeded with 1% of 1B strain fibrils[7]. The samples were loaded in a ThermoMixer (Eppendorf, Hamburg, Germany) in a 24-position 1.5 mL Eppendorf tube holder equipped with a heating lid. Temperature was set to 37 °C, and continuous shaking at 2000 rpm proceeded for 4 days. PFF templating of the fibrillisation products was quality-checked using the fibrilloscope[7].

Sonication of PFFs and LBs

Prior to intracerebral injections, PFF and LB tubes were sonicated at 20 °C in a Bioruptor Plus water bath sonicator (Diagenode, Liège, Belgium) equipped with thermostatic control and automated tube carousel rotator. The sonication power was set to "high", and 10 cycles of 30 s on followed by 10 s off were applied.

Animals and surgical procedures

Eigth-week-old wild-type C57BL/6Jr mice were purchased from Janvier laboratories and reared at the University of Bordeaux animal facilities. Animals were maintained in standard conditions under a 12-h light/dark cycle with water and food provided ad libitum and acclimatised for two weeks before starting the experiments. Before surgery, mice received buprenorphine (0.1 mg/kg) as an analgesic and lidocaine (5 mg/kg) as a local anaesthetic. For surgery, anaesthetised (isoflurane 2%) mice received 2 µL of LBs, PFFs or PBS by stereotactic delivery (400nL/min rate) using a 30-gauge Hamilton syringe connected to a microinjection pump (World

Precision Instruments) to the region immediately above the right substantia nigra (AP-2.9/ML −1.3/DV −4.5). The needle was left in place for 10 minutes to prevent leakage.

SWCNTs preparation and characterisation

SWCNTs solution was prepared following the previously described methods[9] with some minor modifications. 1 mg HiPco synthesised SWCNTs (batch #189.7) was suspended in 0.5% w/v phospholipid-polyethylene glycol (PL-PEG) (#mPEG-DSPE-5000, Nanocs) in 10 mL MQ water. The dispersion was typically homogenised for 15 min at 8000 rpm using a dispersing instrument (IKA T-10 Basic) and then further dispersed by tip sonication at 20 W (output power) for 10 min under the ice. Nanotube bundles and impurities were precipitated by centrifugation at 10621 g for 60 min at room temperature. 70–80% of the supernatant of PL-PEG suspended SWCNTs was then collected and stored at 4 °C. The concentration of the SWCNTs stock solution was estimated by UV (EVOLUTION 220, Thermo Scientific). A range of SWCNTs concentrations have been used (1–10 mg/L). The length of the SWCNTs was measured by AFM. For this, typically, SWCNTs solution was drop-casted on freshly cleaved mica surfaces. Then, the substrate was gently rinsed with water, followed by overnight air drying.

SWCNTs injection and acute brain slice preparation

6 µl of SWCNT solution (1–10 mg/mL) were injected into the right lateral ventricle of living mice by stereotactic surgery (coordinates from bregma: −0.5 mm anteroposterior, 1 mm mediolateral, −2.4 dorsoventral) as previously described[9]. 30 min before surgery, animals received subcutaneously received buprenorphine (0.1 mg/kg) as an analgesic and lidocaine (5 mg/kg) as a local anaesthetic. Surgery was performed under deep isoflurane anaesthesia. SWCNTs solution was injected with a 30-gauge Hamilton syringe coupled to a microinjection pump (World Precision Instruments) at a 1 µl/min flow rate. The needle was left in place for 12 min to avoid leakage, then slowly retracted, stopping for another 2 mins at −1.2 DV.

Between 40 min-1 h after injection of the SWCNTs, mice were euthanised by cervical dislocation. Brains were swiftly extracted, and coronal sections (300 µm thick) were prepared in a VT1200S vibratome (Leica) in ice-cold NMDG solution and left to recover in RT NMDG solution for at least 15 min. NMDG composition in mM: 93 NMDG, 2.5 KCl, 1.2 NaH2PO4.2H20, 20 HEPES, 25 glucose, 30 NaHCO3, 10 MgSO4, 0.5 CaCl2. 1 Sodium Pyruvate and 12 N-acetylcysteine were added just before the experiment. pH was adjusted to 7.3–7.4 using HCl. Measured Osm 290–300. Slices were then transferred to RT aCSF (gassed with 95% O2, 5% CO2) with the following composition (in mM) 140 NaCl, 2.5 KCl, 1.2 NaH2PO4.H2O, 26 NaHCO3, 10 glucose, 10 HEPES, 2 MgSO4 and 2 CaCl2. Sodium Pyruvate and 12 N-acetylcysteine were added just before the experiment. pH was adjusted to 7.3–7.4 using HCl. Osm 300–310.

Near-infrared single-particle microscopy

Acute slices were prepared as described above. After recovery, images were collected at 35 °C in a 3D-printed chamber with controlled temperature by a feedback system. Pre-warmed carbogen-bubbled aCSF was perfused throughout the chamber by a peristaltic pump. Slices were imaged for no more than 45 min. Imaging of moving SWCNTs in the ECS was performed on a customized upright epifluorescent microscope (Nikon). An 845 nm laser diode (QSI), polarised circularly with a quarter-wave plate (Thorlabs), was used to excite the (6,5) SWCNTs at a phonon sideband. Emission light was collected through a 900 nm long-pass filter (Chroma) using a 25x/1.10NA water immersion objective (Nikon). Images were acquired with an InGaAs camera (C-RED 2 – First-Light Imaging) at 33 ms exposure time. A 1.5x zoom magnification was applied to match the camera pixel size with the microscope point-spread function width. Before recording, transmission white light was used to check the position in the entire slice and determine the brain region to be imaged. To avoid non-physiological data acquisition, the first 10 µm of tissue was always discarded to exclude the first cell layer, which was potentially damaged during slicing.

Single-nanotube localisation analysis

The image analysis was performed as previously described with minor modifications[9]. Briefly, individual SWCNTs were super-localized with a 2D Gaussian fit and coordinates were linked to reconstruct individual trajectories. Diffusivities and local ECS dimensions were then extracted as previously described[8] upon drift correction using non-mobile particles in the field of view. For each trajectory, the instantaneous mean square displacement (MSD_{inst}) analysis was used to estimate the instantaneous diffusion coefficient D_{inst}. MSD values were calculated over a sliding window of 10 frames and linear fits were then applied to the first 3 time points to retrieve values of D_{inst}. Immobile SWCNTs, characterised by the plateau shape of their global MSD, were excluded from the analysis. Instantaneous diffusion values have been normalised using an experimentally D_{ref} value calculated from SWCNTs diffusing freely in aCSF, providing a D_{inst}/D_{ref} value reflecting diffusion velocity with respect to the free medium. D_{ref}, the free diffusion constant of the considered SWCNT in a fluid having the viscosity of the cerebrospinal fluid ($1.91 \pm 0.03\ \mu m^2.s^{-1}$) was measured experimentally by measuring the slope of the MSD of freely diffusing SWCNTs in aCSF (See exact composition of aCSF used for measure D_{ref} in "SWCNTs injection and acute brain slice preparation" method). Only moving SWCNTs were analysed. Outliers and analytical artefacts values outside the $0 < D_{inst}/D_{ref} < 0.15$ range were excluded. To estimate local ECS dimensions, the shape of the local area explored by individual SWCNTs along their trajectory was analysed using a 6-point time window[9]. This time window was chosen at maximum confinement (i.e. when the shape of the local area is maximally distorted by local ECS dimension as compared to expected in unconfined environments) as defined by the eccentricity ratio of the ellipse formed by the SWCNT trajectory

Immunostaining and pathology characterisation

Animals were killed by cervical dislocation, and brains were swiftly extracted. Brains were fixed for 72 h in 4% PFA at 4 °C and then kept in 20% sucrose/PBS (24 h) before being frozen by immersion in a cold isopentane bath (−60 °C) for at least 1 min and stored immediately at −80 °C until sectioning in a cryostat at −20 °C. 50 µm-thick coronal sections were collected and kept in Phosphate-buffered saline (PBS1X)-azide 0.2% at 4 °C before immunostaining. For immunohistochemistry, 50 µm free-floating coronal sections were blocked and permeabilised 1 h with 1% BSA + 0.3% Triton X-100 in PBS1X and incubated overnight with an appropriate primary antibody: TH (Rb, clone EP1532Y, ab137869, abcam), Iba1 (Rb, 019-19741, Wako), anti-DARP-32(Rb, clone 19A3, mAb #2306, Cell Signalling) or anti-pS129-α-synuclein (Rb, clone EP1536Y, ab51253, Abcam). Staining was revealed using an anti-rabbit HRP EnVision kit (Dako) for 30 min followed by DAB revelation and counterstained with cresyl violet when necessary. Stereological counting of DARP-32 was performed using the Mercator Pro Software (Explora Nova). Iba-1 surface was calculated using the Visiopham software by threshold analysis. Striatal TH intensity was quantified using imageJ/Fiji software.

Confocal imaging and hyaluronan network analysis

For visualisation of the hyaluronan, matrix slices were blocked following a streptavidin-biotin blocking kit instruction (Vector Labs) for 20 min and incubated overnight with biotinylated-hyaluronic acid binding protein (HABP from bovine nasal cartilage, #385911, Merck-Millipore) diluted in blocking solution. Staining was revealed with Streptavidin-Atto647N (Sigma-Aldrich). When needed, double labelling was achieved by re-blocking samples with 4% normal goat serum and overnight incubation with primary antibodies anti-pS129-α-synuclein (Rb, EP1536Y, ab51253,Abcam). Staining was revealed with appropriate secondary antibodies conjugated with Alexa 488 or 647 (Thermo Fisher). The section was mounted on #1.5 coverslips with VECTASHIELD® Antifade Mounting Medium and left to dry overnight in darkness. Confocal images were acquired in a Leica TCS SP8 microscope with a 63X Plan Apo CS objective with oil immersion, maintaining image acquisition settings (laser power, AOTF, detection parameters) between sessions mage stacks (pixel size: 90 nm, z-step 0.5 µm). We quantified

hyaluronan network complexity by fractal dimension analysis. After thresholding and skeletonisation, the box-counting fractal dimension was calculated using the FractalCount plugin for Fiji/ImageJ using default parameters. Each striatal fractal value was derived from four different micrographs selected to represent the dorsoventral and mediolateral axes.

Statistics and reproducibility

Statistical discrete analyses regarding figures of immunohistochemistry and matrix characterisation were performed using GraphPad Prism 9.0 software: When comparing 3 groups we used the Kruskal Wallis test with post hoc Dunn's multiple comparisons test. Post hoc significative p values are shown in figures. Two-group comparison was done using Mann–Whitney t tests. SWCNTs-related p values were obtained using bootstrapping methods to avoid the artefact where classic p-tests tend to produce extremely small p-values due to the increased power of the test with large sample sizes. We used Python pandas numpy and scipy packages. We used ANOVA tests for overall differences among three groups followed by post hoc pairwise t tests adjusted using the Bonferroni correction. Post hoc significative p values are shown in figures. Bootstrap hypothesis test parameters: alpha = 0.05, number of bootstrap samples = 10,000, sample size = 1000. The figure legends specify the number of replicates (n). Discrete data are presented as mean ± SD unless otherwise stated.

Data availability

The source data for all graphs and charts are available at Zenodo: https://doi.org/10.5281/zenodo.11518921.

Code availability

Customs scripts and software code generated for this paper are available from the corresponding authors upon reasonable request.

Received: 9 June 2024; Accepted: 28 November 2024;
Published online: 30 December 2024

References

1. Masuda-Suzukake, M. et al. Pathological alpha-synuclein propagates through neural networks. *Acta Neuropathol. Commun.* **2**, 1–12 (2014).
2. Lee, H.-J., Bae, E.-J. & Lee, S.-J. Extracellular α-synuclein—a novel and crucial factor in Lewy body diseases. *Nat. Rev. Neurol.* **10**, 92–98 (2014).
3. Soria, F. N. et al. Synucleinopathy alters nanoscale organization and diffusion in the brain extracellular space through hyaluronan remodeling. *Nat. Commun.* **11**, 3440 (2020).
4. Naba, A. Mechanisms of assembly and remodelling of the extracellular matrix. *Nat. Rev. Mol. Cell Biol*. https://doi.org/10.1038/s41580-024-00767-3 (2024).
5. Rike, W. A. & Stern, S. Proteins and transcriptional dysregulation of the brain extracellular matrix in Parkinson's disease: A systematic review. *Int. J. Mol. Sci.* **24**, 7435 (2023).
6. Rosh, I. et al. Synaptic dysfunction and extracellular matrix dysregulation in dopaminergic neurons from sporadic and E326K-GBA1 Parkinson's disease patients. *npj Parkinson's. Dis.* **10**, 38 (2024).
7. De Giorgi, F. et al. Novel self-replicating alpha-synuclein polymorphs that escape ThT monitoring can spontaneously emerge and acutely spread in neurons. *Sci Adv* **6** https://doi.org/10.1126/sciadv.abc4364 (2020).
8. Godin, A. G. et al. Single-nanotube tracking reveals the nanoscale organization of the extracellular space in the live brain. *Nat. Nanotechnol.* **12**, 238–243 (2017).
9. Paviolo, C. et al. Nanoscale exploration of the extracellular space in the live brain by combining single carbon nanotube tracking and super-resolution imaging analysis. *Methods* **174**, 91–99 (2020).
10. Syková, E. & Nicholson, C. Diffusion in brain extracellular space. *Physiol. Rev.* **88**, 1277–1340 (2008).
11. Tønnesen, J., Hrabětová, S. & Soria, F. N. Local diffusion in the extracellular space of the brain. *Neurobiol. Dis.* **177**, 105981 (2023).
12. Soles, A. et al. Extracellular Matrix Regulation in Physiology and in Brain Disease. *Int. J. Mol. Sci.* **24**, 7049 (2023).
13. George, N. & Geller, H. M. Extracellular matrix and traumatic brain injury. *J. Neurosci. Res.* **96**, 573–588 (2018).
14. Bonneh-Barkay, D. & Wiley, C. A. Brain extracellular matrix in neurodegeneration. *Brain Pathol.* **19**, 573–585 (2009).
15. Cabral-Pacheco, G. A. et al. The roles of matrix metalloproteinases and their inhibitors in human diseases. *Int. J. Mol. Sci.* **21**, 9739 (2020).
16. Moretto, E., Stuart, S., Surana, S., Vargas, J. N. S. & Schiavo, G. The role of extracellular matrix components in the spreading of pathological protein aggregates. *Front. Cell. Neurosci.* **16**, 844211 (2022).
17. Sung, J. Y. et al. Proteolytic cleavage of extracellular secreted α-synuclein via matrix metalloproteinases. *J. Biol. Chem.* **280**, 25216–25224 (2005).
18. Crapser, J. D., Arreola, M. A., Tsourmas, K. I. & Green, K. N. Microglia as hackers of the matrix: Sculpting synapses and the extracellular space. *Cell. Mol. Immunol.* **18**, 2472–2488 (2021).
19. Cragg, S. J., Nicholson, C., Kume-Kick, J., Tao, L. & Rice, M. E. Dopamine-mediated volume transmission in midbrain is regulated by distinct extracellular geometry and uptake. *J. Neurophysiol.* **85**, 1761–1771 (2001).
20. Stoll, A. C. & Sortwell, C. E. Leveraging the preformed fibril model to distinguish between alpha-synuclein inclusion-and nigrostriatal degeneration-associated immunogenicity. *Neurobiol. Dis.* **171**, 105804 (2022).
21. Bourdenx, M. et al. Identification of distinct pathological signatures induced by patient-derived alpha-synuclein structures in nonhuman primates. *Sci. Adv.* **6**, eaaz9165, https://doi.org/10.1126/sciadv.aaz9165 (2020).

Acknowledgements

We thank PIV-EXPE colleagues for animal care. We thank François Ichas for providing the PFFs and Morgane Darricau, Remi Kinet, and Ivo Calaresu for helpful discussions. This study received funding from the European Research Council (ERC) under the European Union's Horizon 2020 research and innovation programme (Grant agreement No. #951294) and financial support from the French government in the framework of the University of Bordeaux's IdEx "Investments for the Future" programme/GPR BRAIN_2030. S.N. acknowledges funding from the European Union's Horizon 2020 research and innovation programme under the Marie Skłodowska-Curie grant agreement No. 101024294.

Author contributions

J.E.P., S.N., and Q.G. carried out single-nanotube tracking experiments. S.N. prepared and characterised SWCNTs. J.E.P. and Q.G. performed the SWCNTs analysis. J.E.P., E.D., C.M., M.H.C., and M.L.A. performed immunostainings and confocal imaging. B.D. extracted and purified samples from patients. J.E.P. and E.B. conceptualised and drafted the first version of the manuscript. All authors commented on and approved the final version. L.C. and E.B. secured funding and coordinated the project.

Competing interests

E.B. is the Chief Scientific Officer of Motac Neuroscience Ltd. All other authors declare no competing interests.

Additional information

Supplementary information The online version contains supplementary material available at https://doi.org/10.1038/s41531-024-00850-8.

Correspondence and requests for materials should be addressed to E. Bezard.